The use of segmented cathodes to determine the spoke current density distribution in HiPIMS plasmas

Phitsanu Poolcharuansin[1,2], Francis Lockwood Estrin[1] and James W. Bradley [1, a)]

[1] *Department of Electrical Engineering and Electronics, University of Liverpool, Brownlow Hill, Liverpool L69 3GJ, UK*

[2] *The Technological Plasma Research Unit, Department of Physics, Mahasarakham University, Maha Sarakham 44150, Thailand*

[a)] Author to whom correspondence should be addressed. Email: j.w.bradley@liverpool.ac.uk

Abstract

The localized target current density associated with quasi-periodic ionization zones (spokes) have been measured in a High Power Impulse Magnetron Sputtering (HiPIMS) discharge using an array of azimuthally separated and electrical isolated probes incorporated into a circular aluminum target. For a particular range of operating conditions (pulse energies between 1 and 2 J and argon pressures from 0.5 to 1.5 Pa), strong oscillations in the probe current density are seen with amplitudes up to 60% above a base value. These perturbations, identified as spokes, travel around the discharge above the target in the **E**×**B** direction. Using phase information from the angularly separated probes the spoke drift speeds, angular frequencies and mode number have been determined. During each HiPIMS pulse the spoke velocity is seen to increase, from typically 6.5 km s^{-1} at a time when the total discharge current density approaches its peak value to 10 km s^{-1} at the end of the pulse. Such an observation is consistent with the assertion of Brenning and Lundin (2012 *Phys. Plasmas* **19** 093505) that spoke velocities correspond to the critical ionization velocity (CIV), which changes as the plasma composition changes. The largest fluctuations in the strip probe signal were observed at an argon pressure of 0.68 Pa and pulse energy of 1.79 J. In this particular case, the temporal angular frequencies vary from 3.2×10^5 to 4.5×10^5 rad s^{-1}. From the shape of individual current density oscillations, it appears that the leading edge of the spoke is associated with a slow increase in local current density to the target and the rear with a more rapid decrease. The measurements show that the discharge current density associated with individual spokes is broadly spread over a wide region of the target.

1. Introduction

High power impulse magnetron sputtering HiPIMS is gaining interest from the scientific, engineering and industrial communities as an exciting and potentially valuable physical vapour deposition technique for the production of high-quality functional thin films [1]. At its heart, HiPIMS is a merger of pulse power and conventional magnetron sputtering technologies which facilitates the production of extremely dense (~ 10^{19} m^{-3}), short lived (~ 100 μs) plasmas with a high fraction of the sputtered species arriving as ions at the substrate [2]. With target power densities often up to 10 $kWcm^{-2}$ during the main sputtering phase the typical duty cycles are kept short (~ 1%) to prevent overheating of the device.

HiPIMS systems, as with all sputtering magnetrons, rely on electron trapping in mutually perpendicular electric **E** and magnetic fields **B** to provide high ionisation rates at low operating pressures (~ 0.1-10 Pa) [3]. Typically, with vacuum magnetic fields up to ~ 0.05 T in the magnetic trap, the bulk plasma electrons (of temperature a few eV) can be considered magnetized and therefore execute Hall drifts while the heavy positive ions should be subject only to free fall in the **E** fields to the target. Any component of fast secondary electrons accelerated in the cathode fall, will execute a cycloid motion with radius of curvature typically less than 10 mm and can also be considered magnetised. This principle of intrinsic electron drift has been studied and exploited in other technological plasmas such as homopolar plasmas [4], Hall thrusters [5], and Q–machines [6] and other linear plasma devices [7].

Such configurations, in which considerable azimuthal (Hall) electron current flows against a static background of ions in a closed loop **E**×**B** drift channel, are characterised by a great many inherent plasma oscillations and instabilities over a wide range of frequencies, 10^4 - 10^{10} Hz [8]. These can include, drift wave instabilities [6], modified two-stream instabilities (MTSI) [9] lower-hybrid waves [10], as well as, in some discharge conditions, coherent plasma structures which rotate around the discharge in the Hall **E**×**B** drift channel [11,12].

In HiPIMS, such structures have been observed, and are usually referred to as either bunches [13], spokes [14] or ionization zones [15]. They are believed to be regions of higher local plasma density that rotate along the drift channel in the **E**×**B** direction at speeds consistent with the critical ionization velocity (CIV). This velocity depends on the ionisation potential and mass of the

species forming the majority of ions in the plasma [14]. Experimental determined spoke velocities (in the range 2 - 10 km s^{-1}) for a range of different HiPIMS target materials and sputtering gases agree well with the predicted CIV speeds [16] and are always about an order of magnitude lower than the **E**×**B** electron drift speed [15]. With closed loop distances around the racetrack of several tens of cm's and typical mode numbers m of the instabilities observed from m = 1 to 4, the speeds of such structures correspond to frequencies of several 100's kHz [17,18].

To study and characterize the detailed nature of spokes in HiPIMS discharges a number of diagnostic techniques have been employed. These include the use of fast intensified cameras (ICCD's) to determine their shape, mode number, wavelength, rotation speed, and the general conditions of existence for such rotating instabilities [8,13,15,17–21]. Other non-perturbing optical techniques including two fiber optical monitoring [18] and optical emission spectroscopy [19] have been used to both observe spoke motion and learn more about the composition of emitting species including Al I, Al II, Ar I and Ar II.

Electrical probes, operating in either the electron or ion saturation current regions of the characteristic, positioned in the magnetic trap have been used to observe the modulation in the plasma density as spokes intercept the probe [13,22]. Such probes, of varying geometry, have also been used in more remote positions to detect long range signatures of the spokes [23]. Electrically isolated [18,22] and emissive probes [15] have been used to determine the local fluctuation of the floating and space potentials due to the presence of spokes. However, in some cases the probes themselves can perturb the plasma under observation.

The existence of spokes has been linked to observations of enhanced ion energies in HiPIMS. Using energy-resolved mass analyzers a number of studies have shown that when such instabilities exist in the plasma (seen by probe detection), there are pronounced extensions in the energy of post-ionized sputtered species arriving at the substrate [24,25] but also remarkably in directions tangential the target [23].

These observations have led to the idea that associated with the spokes there must be a region of more positive plasma potential (i.e. a potential humps of 10–50 V) generated by regions of

differing space charge. This potential structure can accelerate ions (created in the spoke) to higher energies in all directions away from the target [24,25] however enhanced in the direction of spoke rotation [23], with the positive potential structure of the spoke acting like an impenetrable moving wall to on-coming ions [14].

Conditions for the existence of spokes has been investigated as a function of discharge current [26], applied power [21], target power density [24], and pressure [18]. It is found that the mode number m decreases with increased power until a threshold is reached after which no spokes can be identified [21]. Increasing pressure slows the spokes velocity [18].

To prevent a discontinuity of electric potential around the racetrack the spoke itself must consist of two adjacent double layers [27] (actually a triple layer structure as seen in other types of plasmas [28]). Such layers consist of three regions of alternating space charge polarity, with a reversal in the internally generated azimuthal electric field components $\mathbf{E}_\theta$. These E-fields cross with the vacuum **B**-field to produce electron drifts across the magnetic field lines, perpendicular to the plane of the spoke motion [14]. This phenomenon has been observed using streak cameras [15,29] as the creation of electron flare or jets emanating from the center or possibly the leading edge of the spoke, a region of the spoke where $\mathbf{E}_\theta$ points in the $\mathbf{E}\times\mathbf{B}$ direction [27]. It is conjectured that these flares can carry away a substantial part of the total electron current eventually reaching the grounded walls. Using segmented anodes in a Hall thruster device the electron return current associated with a single spoke was found to be over 50% of the total discharge current [30]. Such cross-field electron transport has been associated with the mechanisms behind anomalous electron diffusion seen in Hall thrusters [31]; appropriate to all $\mathbf{E}\times\mathbf{B}$ devices which can drive axial two-stream instabilities [14].

In the triple layer model advocated in [24,25] and updated recently by [27] the azimuthal electric field must also reverse and so azimuthally drifting electrons in the $\mathbf{E}\times\mathbf{B}$ channel entering the rear of the spoke will be directed towards the cathode [27], however, overall the net electron drift from all regions of the target must be to the anode of course. This drift was observed in a PIC–MCC simulation model of a concentric cylindrical homopolar plasma by Boeuf and Chaudhury [12].

Since it believed spokes are high density regions with higher associated ionization rates it is logical to assume that in HiPIMS (as well as other similar discharges) they give rise to a considerable fraction of the total measured discharge current. This was assumed in the calculations of ion current to the target from spokes in [13] as well as the basis for the electron current flowing in the opposite direction towards ground (vessel walls) through flare formation [25] as discussed above.

Plasma parameters such electron temperature and density associated with the spokes have been obtained in Hall Thrusters [30] using flush mounted planar probes, however, such measurements with electrical probes in HiPIMS are problematic, for instance they can potentially destroy the phenomena to be measured, and the probes themselves can accumulate a considerable amount of deposit on the tips, corrupting their operation. Here we do not attempt to measure the plasma parameters within spokes themselves, however employ an array of electrical probes (strips) forming a segmented target to measure directly the distribution of current sourced from individual spokes as they rotate around the racetrack. The strip probes, made of the target material, were mounted flush to the target surface, making them indistinguishable from the rest of the target as far as the plasma is concerned. Using this arrangement, we also measure the spoke velocities, mode number and azimuthal profile (shape) during the HiPIMS pulse.

2. Experimental setup

All experiments were conducted in a purpose-built cylindrical vacuum vessel, 300 mm in length and 260 mm in diameter, pumped down to a base pressure of 6.5×10^{-4} Pa using a turbo molecular pump backed by a rotary pump. Argon was introduced into the vessel with flow rates ranging from 4 to 32 sccm (standard cubic centimeter per minute) to vary the operating pressure between 0.27 Pa – 2.4 Pa. The operating pressure and flow rates were determined and controlled using a capacitance pressure gauge (MKS 628A) and a mass flow controller (MKS 1179A), respectively. The general chamber configuration is shown in figure 1a.

The magnetron used in this study was a circular unbalanced type, equipped with a 75 mm diameter aluminum target of 5.53 mm thickness and 99.995% purity. The magnetic field strength on the target surface at the center of the racetrack (21.5 ± 0.5 mm radius) was ~ 80 mT.

To strike HiPIMS plasmas an in-house built power supply was used, providing a peak current of 60 A [32]. In this study the supply was operated at a repetition rate of 3 Hz and a pulse width of ~ 70 μs providing energies up to 2.15 J per pulse.

In order to measure the target current locally as the spokes rotate above it, the target was segmented, with the introduction of three 2.14 ± 0.02 mm wide flush-mounted aluminum strip probes (same purity as the target) placed in machined slots at 3 angular positions (45^o from each other) around the target, see figure 1b. The three strip probes filled the entire target radius and extended past the target edge by 5 mm to allow electrical connections. The stripe probes were electrically isolated from the rest of target by a thin layer of polyimide tape of thickness of 0.07 ± 0.01 mm, placed around 3 sides of the probe, it provided a tight fit. This insolation thickness defined the gap w_{gap} between the strip probe and the target.

We argue that, from a plasma perspective, the stripe probes are indistinguishable from the rest of the target provide w_{gap} is smaller than both the cathode sheath thickness s and the gyro-radius r_{eL} of bulk electrons and secondary electrons emitted from the target. From the literature [33], we can take the electron densities and temperatures close to the target to be $n_e \sim 10^{19}$ m^{-3} and $(k_B T_e)/e \sim$ 3 eV respectively. With a cathode fall voltage of $V_0 \sim 500$ V and magnetic field strength B ~ 80 mT we calculate s ~ 0.15 mm [34] and $r_{eL} \sim 0.94$ mm [35], satisfying the conditions $w_{gap} < s$ and $w_{gap} < r_{eL}$. The gyro radii of high-energy electrons accelerated to a fraction of the cathode fall potential ($>> kT_e$) will strongly satisfy the condition $w_{gap} < r_{eL}$.

The three strip probes were connected directly the power supply as shown in figure 1b. In this configuration they always remained at the same potential as the target, but with their contribution to the total current measured separately using Pearson current probes (Model 2877 with 1V/A). The total target current, I_d, was measured using a larger Pearson probe (Model 3972 with 0.1V/A). The four current waveforms were recorded using a digital oscilloscope (Tektronix DSP 3030D with 300 MHz bandwidth) in a single short mode if not otherwise stated. The discharge voltage waveforms V_d were measured separately using a high voltage probe (Tektronix P5100).

The area of each individual strip probes and whole target (including the probes) were calculated to be $A_p \sim 0.61$ cm^2 and $A_d \sim 44.18$ cm^2 respectively. Together with the measured currents from

the strips I_p and the total target current I_d it is possible then to determine the respective current densities j_p and j_d. However, to accurately compare j_p and j_d (as we do in the first part of section 2), it is important that these measurements agree in "spoke-free" conditions. Since the strip probes are rectangular in shape and inserted into essentially circular geometry and that they overhang the target at the edges to allow electrical connections, we cannot guarantee any "ridged body" plasma structure moving above them will see exactly the same proportion of their entire areas A_p and A_d. So, to effectively calibrate the strip probes, we ran the magnetron over a range of DC conditions (p_{Ar} = 0.78 Pa, 100 W < power < 300 W) in which no spokes were observed, and calculated the current densities j_p and j_d. This provided us with an effective area ratio of $A_p/A_d \sim 0.0170$, 20 % higher than the geometric areas. One such note that although no spokes were observed here in DC conditions, the signature of spokes have indeed been detected in DC sputtering elsewhere [36] . The conditions required to generate spokes in non-HiPIMS plasmas are yet to be properly investigated.

Since the strip probes were isolated from the target, effective cooling of the probes over long durations was problematic. To prevent overheating of the probes we used a very low frequency of 3 Hz, while still applying high peak powers. With low associated duty cycles it was necessary to use an auxiliary pre-ionizer source [32] in conjunction with the HiPIMS unit to easy breakdown on each new pulse. Measurements of j_p taken at the beginning and end of long periods of operation showed no differences, indicating that if any overheating did occur, it did not affect the results.

3. Results and Discussion

Figure 2 shows simultaneous measurements of the current density at a strip probe j_p and the current density to the whole target (which includes the strip probe) j_d. We have restricted ourselves to observations in the driven phase of a number of different HiPIMS discharges for a variation of pulse energies E_p (0.15 to 2.2 J) and gas pressures p_{Ar} (0.18 to 1.59 Pa). For this particular part of our investigations, it was necessary to use the effective area ratio calibration as described in section 2.

The data was obtained using the probe marked at angle $\theta = 0$ in figure 1b. Under certain conditions we observe strong oscillations in j_p which we attribute to the existence of coherent spoke structures. At the low pressures ($p_{Ar} = 0.18$ Pa) and low pulse energies ($E_p < 0.5$ J), oscillations appear somewhat chaotic with irregular and non-periodic peaks and valleys during the pulse. However, as the discharge energy is increased more coherent periodic structures develop with oscillation amplitudes growing monotonically with E_p. There appears to be a threshold in E_p for coherent spokes to form that decreases with increases in pressure. For example, in figure 2b and 2c we see at $p_{Ar} = 0.81$ Pa a threshold value of $E_p \sim 1$ J, however this decreases to $E_p = 0.6$ J at = 1.59 Pa.

The largest amplitude in the j_p oscillations (seen at $E_p = 1.8$ J, $p_{Ar} = 0.81$ Pa) is about 45% above the base level (the j_p values of in the valleys) at 30 - 40 μs into the pulse (figure 2b). In contrast to the strip probe measurements, the total discharge current density j_d measurements at any operating condition show little or no perturbations. This can be expected, since the current contribution from any non-changing structure moving around the whole target will yield no temporal dependency in the I_d measurement. The very small oscillations seen in j_d, discernable in figure 2b and reported in the discharge current elsewhere [24], may be due to the temporal evolution of the spoke plasma parameters in the frame of reference rotating with the spokes. Although we have no optical imaging evidence for spokes in this study, the lack of oscillations in j_d but strong oscillations in the j_p measurements gives us confidence we are observing moving plasma structures passing over our strip probe and not any kind superimposed signal from the plasma-power supply network.

To illustrate that the presence of spokes is conditional on the discharge energy E_p and to allow us to see in detail the form of the j_p oscillations, measurements for three discharge conditions have been made and are shown in figure 3. Here we choose pulse energies E_p of 0.11, 0.87 and 2.20 J at a single operating pressure of $p_{Ar} \sim 1.30$ Pa.

During the early part of the pulse at low pulse energy, ($t < 30$ μs, $E_p = 0.11$ J) we see no signature of spokes in the j_p traces. This is in agreement with fast imaging evidence from other HiPIMS plasmas operating in similar conditions[20]. However, as the current increase even at this low pulse

energy, we can observe a fluctuation in the strip current waveform from about 40 μs to 65 μs [20]. Increasing the pulse energy to E_p = 0.87 J reveals strong oscillations in j_p. It also seems clear that in the early part of the pulse (i.e. at low discharge current) the plasma is homogeneous, which has been seen elsewhere [20]. Here, strong oscillations in j_p start at t ~ 15 μs and remains throughout the pulse. In figure 3 the dashed lines represent an effective oscillation envelop within which the peak-to-valley amplitude of the oscillation Δj_p, can be determined. We define the bottom of the valley as the base current j_b. For example, at t ~ 40 μs, $\Delta j_p \sim 0.39$ A cm^{-2}, which corresponds to about 32% of the base current density ($j_b \sim 1.20$ Acm^{-2}). The ratio $\Delta j_p/j_b$ varies during the pulse, rising to a plateau of ~ 0.32 at t ~ 40 μs, persisting up to the end of the pulse. At the highest pulse energy condition, $E_p \sim 2.20$ J, oscillations are significantly attenuated with $\Delta j_p \sim 0$, particularly during times of peak discharge current I_d (t ~ 30–40 μs).

The peak-to-valley strip probe current densities normalized to the base current (valley) $\Delta j_p/j_b$ are shown in figure 4. The measurements were obtained at one particular time during the pulse (t ~ 40μs) and are mapped out as a function of pulse energy and operating pressure. The maximum value of $\Delta j_p/j_b$ is ~ 0.6 at $E_p \sim 1.60$ J and $p_{Ar} \sim 0.7$ Pa. In figure 4, we represent an approximate boundary which separates two regions, one where spokes appear to be chaotic and one where they are coherent. It is at low E_p (typically < 1 J) where chaotic behavior is generally observed as reported by Winter et al [8].

One should note that due to limitations in the power supply some operating parameters could not be attained and these are represented by the shaded region in figure 4. Despite this experimental limitation the contour plot does clearly reveal regions where spokes are chaotic, coherent and non-existent. Our observations are in general agreement with those obtained using fast optical imaging [21] to investigate spoke structural evolution.

The mechanism determining spoke formation is unknown but it appears that at low power only chaotic structures are observed and their amplitude is largely independent of pressure. However, once coherent spokes are created pressure plays a key role in determining the current oscillation amplitude above its base value. It is argued that collective behavior such as spoke formation is a result of insufficient ion production, with structures moving to seek regions of enhanced ionization [15]. At high powers, sufficient ionization takes place and spoke structure is lost.

Individual spokes may merge to form a single continuous structure [21], possibly maintaining a reversal in axial electric field (potential fill) but with no azimuthal component. Increased pressures may provide the necessary sustainment and hence reduced spoke current amplitudes.

To gain information on the speeds of the spokes and their mode number j_p measurements were made simultaneously at three strip probes at $\theta = 0$, $\pi/4$ and $\pi/2$. An example taken for the case $E_p \sim 1.79$ J and $p_{Ar} \sim 0.68$ Pa is shown in Figure 5. The j_p waveforms have been stacked (with a vertical increment of $j_p = 1$ Acm^{-2}) to allow the phase information to be seen clearly. The j_p oscillations between probes are coherent in terms of shape, amplitude and period but phase shifted (a time lag τ) with increasing θ. This demonstrates the existence of essentially coherent (and rigidly-formed) current perturbations, (ionization zones) rotating in the anticlockwise **E**×**B** direction. In the particular case chosen, over the driven part of the discharge, we can identify seven distinct oscillation packages as labelled I to VII in figure 5. To calculate the spoke angular frequency, ω and tangential speed, *v* at the racetrack center (radius $r_c \sim 21.5 \pm 0.5$ mm) average time delays τ_{avg} in the peaks have been used. We define $\tau_{avg} = (\tau_{AB} + \tau_{BC})/2$, where τ_{AB} and τ_{BC} is the time delay between probes A and B and probes B and C, respectively. The spoke speed calculations are summarized in table I.

From the average period of oscillation T_{avg} and the time lag τ_{avg} data the mode number m can be determined as $m = (2\pi\tau_{avg})/(\Delta\theta T_{avg})$. In our chosen operating condition ($p_{Ar} \sim 0.68$, $E_p \sim 1.79$ J), we find values of m between 2.8 and 3.1 giving us confidence that we have m = 3.

It is known from the literature that the mode number may vary with operating conditions, for instance with higher m observed for increased pressure (for Ti) [18], increasing from m = 1 to a more fragmented situation with m > 4. The mode number tends to decrease with increasing discharge current as seen in the sputtering of Mo [21] and Al [20] targets. Over all the conditions in this study we find predominately m = 3. At certain conditions the m = 4 can be identified (for instance at $p_{Ar} = 1.6$ Pa and $E_p = 0.8$ J). We do not observe the large m = 1 structure even at low powers (when spokes exist) as observed with Al targets elsewhere [22].

It is interesting that in similar conditions to ours ($p_{Ar} = 0.27$ Pa and $j_d > 1.8$ A cm^{-2}) with an Al target the m = 4 mode rather than m = 3 is seen [20]. More work is needed to understand the form of rotating spoke patterns and their link to discharge conditions.

The tangential speeds shown in Table I, lying between 6.95 and 9.79 km s^{-1} agree well those seen in other HiPIMS discharges with Al targets [15]. We observe that for conditions when spokes actually occur, their speed increases during the HiPIMS pulse, for instance from ~6.95 km s^{-1} (t ~ 22–30 μs) to ~9.76 km s^{-1} (t ~ 56–60 μs) as seen in figure 5 for E_p ~ 1.79 J and p_{Ar} ~ 0.68 Pa.

To determine any gross trends in the spoke speed *v* during the evolving HiPIMS pulse, the speed of individual spokes has been calculated over ten identical HiPIMS pulses and plotted as a function of time in figure 6. This has been done for only one discharge operating condition (E_p ~ 1.79 J and p_{Ar} ~ 0.68 Pa) but the same trends are seen at different conditions for which spokes exist.

We see that as the pulse progresses *v* increases from about 6.5 to 10 km s^{-1}. This increase can partly be understood from a change in composition of the plasma. It is postulated that spoke speeds adhere to the critical ionization velocity CIV hypothesis [16], with the CIV speed given by $v_{CIV} = \sqrt{\frac{2eU_i}{m_n}}$, where U_i is the ionization potential and m_n is the mass of the species being ionized with *e* the elementary charge. As the discharge builds up and certainly at times close to the peak discharge current we expect the discharge to be dominated by Al giving a CIV velocity $v_{CIV,Al}$ = 6.5 km s^{-1}. However towards the end of the pulse we conjecture that argon replaces the Al particles and the CIV velocity will therefore increase to $v_{CIV,Ar}$ = 8.7 km s^{-1}. The results in figure 6 suggest such a trend as the weighted mass m_n and effective U_i value change with composition. The CIV limits for the two species are shown in figure 6. For times greater than 50 μs our calculated spoke velocities exceed the CIV velocity for Ar. One possible explanation for this is that as the spoke evolves in time its' average radial position (as well as shape) may change. If the spokes average radius (correlated with the position of maximum current) were to reduce by about 3 mm our calculated velocities would always be limited to $v_{CIV.Ar.}$ Our estimated spoke velocities compare well to those obtained in other HiPIMS plasmas with Al targets, for instance a velocity of 8.1 ± 0.3 km s^{-1}determined by fast camera imaging [15].

This argument of changing composition is consistent with measurements made using time-resolved tunable diode-laser adsorption [37], where Ar depletion was found to occur at the peak of the target current. In the early stages of the discharge it is difficult to identify and then calculate

spoke speeds, so we are unable to demonstrate that spoke speeds are consistent with the $v_{CIV.Ar}$ velocity as we would expect this stage in the discharge before Al becomes the dominant species.

From observation of the time profile in j_p (as a spoke passes over a probe) useful information on the spoke structure can be obtained. From figure 5 taking a representative spoke (peak II at probe position $\theta + \pi/2$) between 30 and 35 μs we see at the front of the spoke there is a relatively slow two-stage rise in j_p (slew rates ~7.8×10^4 and ~3.5×10^5 A cm^{-2} s^{-1}) to a peak value followed a more rapid fall (~6.7×10^5 A cm^{-2} s^{-1}). This profile is wholly consistent with an elongated (triangular) shape as reported in the literature for spokes above an aluminum target [20,22] in which the apex of the spoke is pointed in the **E**×**B** direction, followed by a sharp trailing edge. This edge is aligned with the direction of the radial magnetic field lines, connecting the inner and outer magnetic pole pieces. This profile also fits with electrical probe data of the signatures of spokes [22] where the bulk of the evidence suggests that spokes are characterized by a gradual rise (in density, potential, current) in the leading edge but a faster decrease at the rear.

Inspection of figure 5 shows very little gap (or time lags) between individual spokes. It was expected that we would see a considerably lower current density between discrete spokes representing a background of weaker homogeneous plasmas. It appears however that the spoke structures are smeared out in the azimuthal direction almost merging nose-to tail but with each spoke characterized by a region of high current densities (40-50% higher than at the periphery of the spokes).

To demonstrate this we have attempted to display the current density data in 2D as done for optical signals obtained from fast imaging. This can be achieved by transforming the temporal distribution j_p (t) to an angular distribution $j_p(\theta)$ and convolving it with a Guassian radial distribution to artificially add radial information. We choose a Guassian function $G(r) = A \exp(-(r-r_0)^2/L^2)$, where r_0 (= 21.5 mm) is the radius of racetrack center, L (= 10 mm) is an assumed mean radial width of the spokes, and A is a scaling constant to be calculated. Although we have no radial measurements of j_p in this study, the invoked Guassian representation of $j_p(r)$ centered on the middle of the racetrack [38] is sufficient to produce a realistic 2-D distribution of target current density $j(\theta, r)$, as shown in figure 7. Here we chose the current density data from figure 5

(probe at $\theta + \pi/2$) over one period T from 30 to 47 μs. To ensure our function $j(\theta, r)$ provides the correct measured discharge current I_d it must satisfy the condition

$$\iint_{0,0}^{2\pi,R} j(\theta,r) r \, d\theta \, dr = I_d$$

Where $j(\theta, r) = G(r)j_p(\theta)$ and R is the target radius. Here the target current I_d is averaged over the same time period ($30 \leq t \leq 47$ μs) as the $j_p(t)$ was collected. Performing the integral yielded, in the particular case chosen, a scaling constant A = 1.3.

It is interesting that in figure 7 our constructed map of $j(\theta, r)$ is very much consistent in form to optical emission fast imaging [20,22]. However due to the lack of real radial information it cannot reproduce for instance a triangular form to the spoke as often seen optically. It seems clear however that spokes do carry a considerable fraction of the discharge current since their elongated structure occupies and significant area of the target in the racetrack region. In the case displayed the peak current density at the spokes center is highly localized and has a current density ~ 43 % greater than that in the racetrack minimum. Future studies using radial separated target probes will yield accurate radial information allowing accurate 2D current density maps to be constructed.

4. Conclusions

Using a segmented target the current densities associated with rotating spokes in a HiPIMS discharge have been investigated. Spokes are identified as regular perturbations in local discharge current density with peak values up to 50 % higher than the valley currents. Generally, as the energy of the HiPIMS pulse is increased the spokes change their nature, moving from chaotic behavior to form coherent regular structures. At our highest pulse energies spokes are extinguished and may form a single continuous structure.

The spokes have been found to have an elongated leading edge and sharper trailing edge, and travel with velocities increasing from 6.5 to 10 km s^{-1} as the HiPIMS pulse develops. These velocities are consistent CIV predictions.

The time signature of spoke current densities show that spokes are effectively smeared out to cover a larger area of the racetrack leaving no discrete gaps in between them. Assuming a realistic radial distribution of current density, a 2D map of the target current density $j(\theta,r)$ has been constructed, showing a general distribution consistent with fast optical imaging of spokes in other studies.

Further investigations using our method is planned to include the use of radially distributed segments to provide information of the radial current density distribution. In addition, the combined use of fast optical imaging and target probes will allow advances in the understanding of spoke creation and sustainment for a variety of different target materials.

Acknowledgements

Phitsanu Poolcharuansin acknowledges support by Mahasarakham University, Thailand and University of Liverpool, UK for his short-term postdoctoral fellowships. Francis Lockwood Estrin would like to thank the University of Liverpool for his studentship funding, as part of the Engineering and Physical Sciences Research Council (EPSRC) Fusion Doctoral Training Network EP/K504178/1. He also wishes to thank the STFC, AsTEC Group, Daresbury, UK for their funding support and Dr. Reza Valizadeh and Dr. Oleg Malyshev of the same for their advice and encouragement.

Figure Captions

Fig. 1: Schematic diagrams of (a) the magnetron and chamber set-up and (b) the strip probes and current measuring arrangements.

Fig. 2: (a), (b) and (c) time traces of the current density, j_p, measured by a strip probe, (d), (e) and (f) time traces of the total target current density, j_d, for a number of pulse energies E_p and argon pressures, p_{Ar} of 0.18, 0.81 and 1.59 Pa.

Fig. 3: The strip probe current densities j_p for a number of pulse energies at p_{Ar} = 1.30 Pa. The marked envelop (dashed lines) is used as a guide to calculate the amplitude (Δj_p) of the oscillation in j_p above the running minimum value j_b.

Fig. 4: A contour plot of $\Delta j_p/j_b$, the ratio of Δj_p normalized to the base current density j_b, at time t = 40 μs for a range of pulse energies E_p and argon pressures p_{Ar}. The hatched region represents an area inaccessible to experiment due to power supply limitations. The dotted line represents the approximate boundary between chaotic and coherent spoke behavior.

Fig. 5: The strip probe current density time traces for E_p = 1.79 J and p_{Ar} = 0.68 Pa. The traces are stacked (incremented by 1 A cm^{-2} to allow the phase relationship to be seen). The rapid, short-lived, negative current observed at the end the pulse is thought to be the result of finite inductance of strip probe assembly and connecting lines.

Fig. 6: A plot of spoke velocities through a HiPIMS pulse, calculated from the time lags in the waveforms between the azimuthally separated strips. The data was recorded over ten HiPIMS pulses for E_p = 1.79 J and p_{Ar} = 0.68 Pa. The target current and voltage for this discharge are also shown.

Fig. 7: A 2D reconstruction of the target current density using measured azimuthal data combined with an assumed Guassian radial current density distribution, of the form $G = A \exp(-(r-r_0)^2/L^2)$. The azimuthal data was obtained for $p_{Ar} \sim 0.68$ Pa, $E_p \sim 1.79$ J, and for spokes passing a single strip in the time period 30 - 47 μs.

Table I: The time lags between neighboring strips τ_{AB}, τ_{BC} and their average value τ_{avg}, angular frequency ω and the tangential speed v at the racetrack center for each ionization zone identified in figure 5.

References

[1] D. Lundin and K. Sarakinos, *J. Mater. Res.* **27**, 780 (2012).

[2] J.T. Gudmundsson, N. Brenning, D. Lundin, and U. Helmersson, *J. Vac. Sci. Technol. A Vacuum, Surfaces, Film.* **30**, 030801 (2012).

[3] A. Anders, *Surf. Coatings Technol.* **205**, S1 (2011).

[4] P.B. Barber, D. a Swift, and B. a Tozer, *J. Phys. D. Appl. Phys.* **5**, 693 (1972).

[5] V. V Zhurin, H.R. Kaufman, and R.S. Robinson, *Plasma Sources Sci. Technol.* **8**, R1 (1999).

[6] H.L. Pecseli, T. Mikkelsen, and S.E. Larsen, *Plasma Phys.* **25**, 1173 (1983).

[7] A.E. Shumack, H.J. de Blank, J. Westerhout, and G.J. van Rooij, *Plasma Phys. Control. Fusion* **54**, 125006 (2012).

[8] J. Winter, A. Hecimovic, T. de los Arcos, M. Böke, and V. Schulz-von der Gathen, *J. Phys. D. Appl. Phys.* **46**, 084007 (2013).

[9] D. Lundin, P. Larsson, E. Wallin, M. Lattemann, N. Brenning, and U. Helmersson, *Plasma Sources Sci. Technol.* **17**, 035021 (2008).

[10] D. Lundin, U. Helmersson, S. Kirkpatrick, S. Rohde, and N. Brenning, *Plasma Sources Sci. Technol.* **17**, 025007 (2008).

[11] E.Y. Choueiri, *Phys. Plasmas* **8**, 1411 (2001).

[12] J.P. Boeuf and B. Chaudhury, *Phys. Rev. Lett.* **111**, 1 (2013).

[13] A. V. Kozyrev, N.S. Sochugov, K. V. Oskomov, a. N. Zakharov, and a. N. Odivanova, *Plasma Phys. Reports* **37**, 621 (2011).

[14] N. Brenning, D. Lundin, T. Minea, C. Costin, and C. Vitelaru, *J. Phys. D. Appl. Phys.* **46**, 084005 (2013).

[15] A. Anders, P. Ni, and A. Rauch, *J. Appl. Phys.* **111**, 053304 (2012).

[16] N. Brenning and D. Lundin, *Phys. Plasmas* **19**, 093505 (2012).

[17] A.P. Ehiasarian, A. Hecimovic, J. Winter, T.D.L. Arcos, R. New, V.S. Der Gathen, and M. Böke, *IOP Conf. Ser. Mater. Sci. Eng.* **39**, 012012 (2012).

[18] A.P. Ehiasarian, A. Hecimovic, T. de los Arcos, R. New, V. Schulz-von der Gathen, M. Böke, and J. Winter, *Appl. Phys. Lett.* **100**, 114101 (2012).

[19] J. Andersson, P. Ni, and A. Anders, *Appl. Phys. Lett.* **103**, 054104 (2013).

[20] A. Anders, *Appl. Phys. Lett.* **100**, 224104 (2012).

[21] T.D.L. Arcos, V. Layes, Y.A. Gonzalvo, V.S. Der Gathen, a Hecimovic, and J. Winter, *J. Phys. D. Appl. Phys.* **46**, 335201 (2013).

[22] a Hecimovic, M. Böke, and J. Winter, *J. Phys. D. Appl. Phys.* **47**, 102003 (2014).

[23] M. Panjan, R. Franz, and A. Anders, *Plasma Sources Sci. Technol.* **23**, 025007 (2014).

[24] C. Maszl, W. Breilmann, J. Benedikt, and a von Keudell, *J. Phys. D. Appl. Phys.* **47**, 224002 (2014).

[25] A. Anders, M. Panjan, R. Franz, J. Andersson, and P. Ni, *Appl. Phys. Lett.* **103**, 144103 (2013).

[26] T.D.L. Arcos, R. Schröder, Y.A. Gonzalvo, V.S. Der Gathen, and J. Winter, *Plasma Sources Sci. Technol.* **23**, 054008 (2014).

[27] A. Anders, *Appl. Phys. Lett.* **105**, 244104 (2014).

[28] G. Petraconi and H.S. Maciel, *J. Phys. D. Appl. Phys.* **36**, 2798 (2003).

[29] P. a. Ni, C. Hornschuch, M. Panjan, and A. Anders, *Appl. Phys. Lett.* **101**, 224102 (2012).

[30] C.L. Ellison, Y. Raitses, and N.J. Fisch, *Phys. Plasmas* **19**, 013503 (2012).

[31] G.S. Janes, *Phys. Fluids* **9**, 1115 (1966).

[32] P. Poolcharuansin, B. Liebig, and J. Bradley, in *IEEE Trans. Plasma Sci.* (2010), pp. 3007–3015.

[33] A. Anders, J. Andersson, and A. Ehiasarian, *J. Appl. Phys.* **102**, 113303 (2007).

[34] A.J.L. Michael A. Lieberman, *Principles of Plasma Discharges and Materials Processing* (John Wiley & Sons, Inc., 2005).

[35] A. Rauch and A. Anders, *Vacuum* **89**, 53 (2013).

[36] A. Anders, P. Ni, and J. Andersson, *IEEE Trans. Plasma Sci.* **42**, 2578 (2014).

[37] C. Vitelaru, D. Lundin, G.D. Stancu, N. Brenning, J. Bretagne, and T. Minea, *Plasma Sources Sci. Technol.* **21**, 025010 (2012).

[38] G. Clarke, A. Mishra, P.J. Kelly, and J.W. Bradley, *Plasma Process. Polym.* **6**, S548 (2009).

Figures

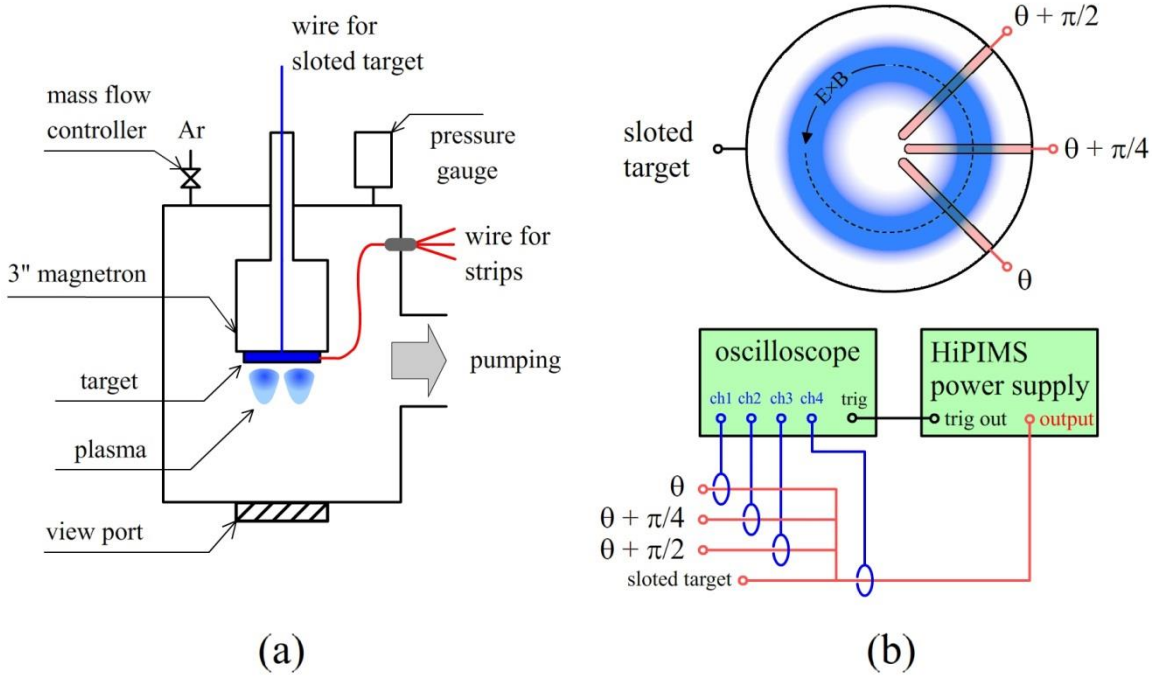

Figure 1.

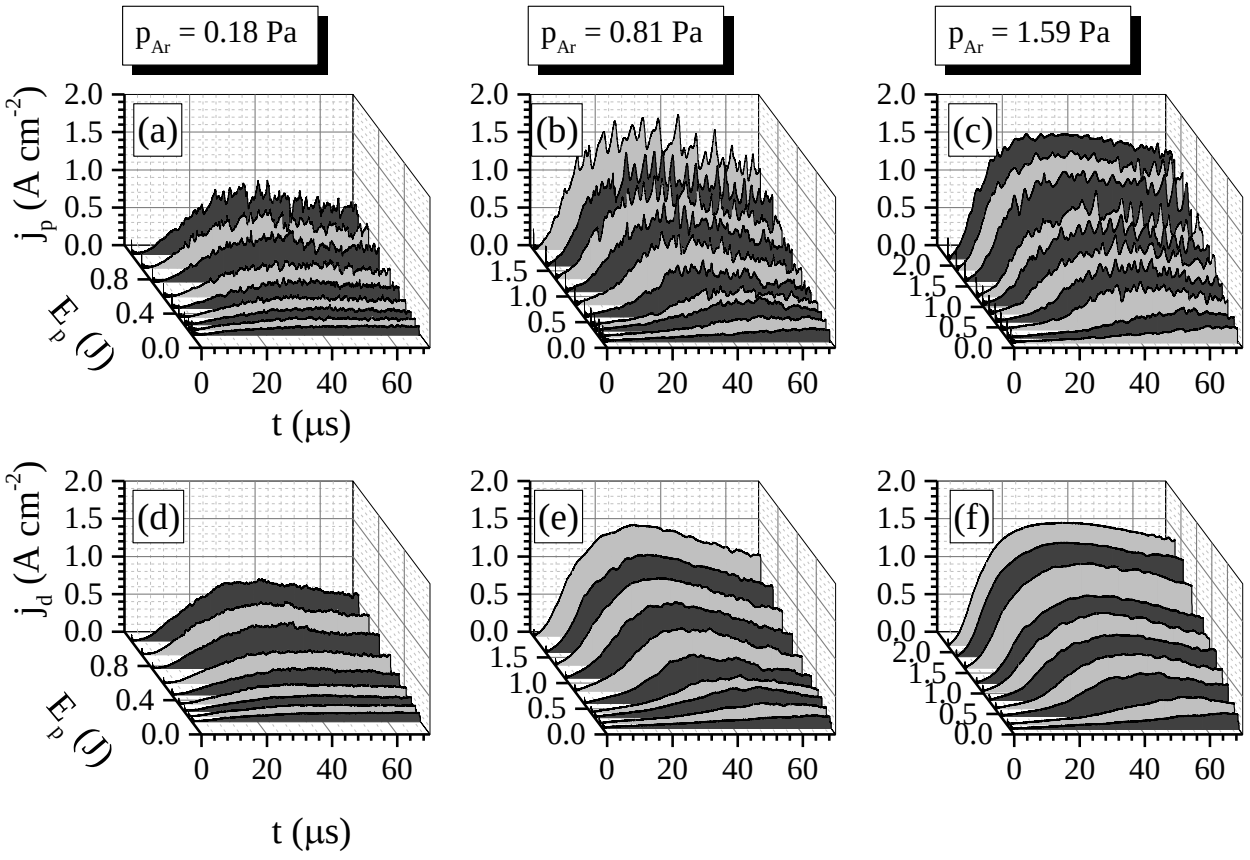
p_Ar = 0.18 Pa
p_Ar = 0.81 Pa
p_Ar = 1.59 Pa
(a)
(b)
(c)
(d)
(e)
(f)
j_p (A cm^-2)
j_d (A cm^-2)
E_p (J)
t (μs)
0.0
0.5
1.0
1.5
2.0
0.4
0.8
0
20
40
60

1

2 Figure 2.

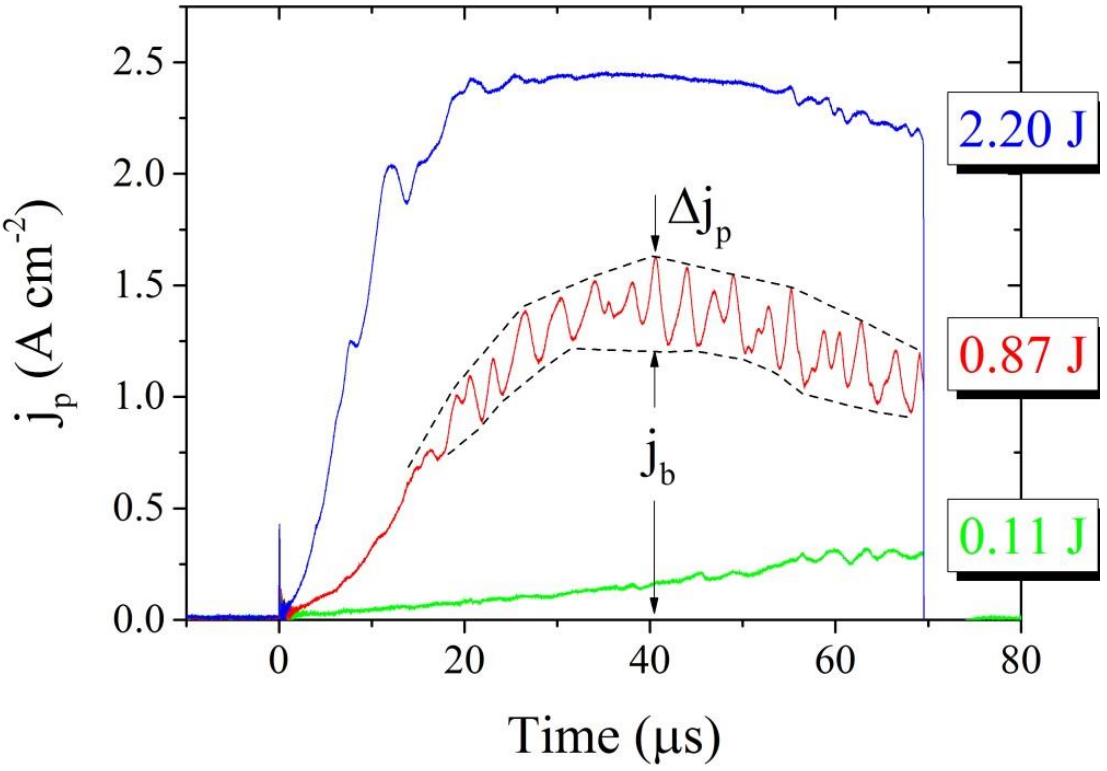
2.5
2.0
1.5
1.0
0.5
0.0
j_p (A cm^{-2})
0
20
40
60
80
Time (μs)
Δj_p
j_b
2.20 J
0.87 J
0.11 J

Figure 3.

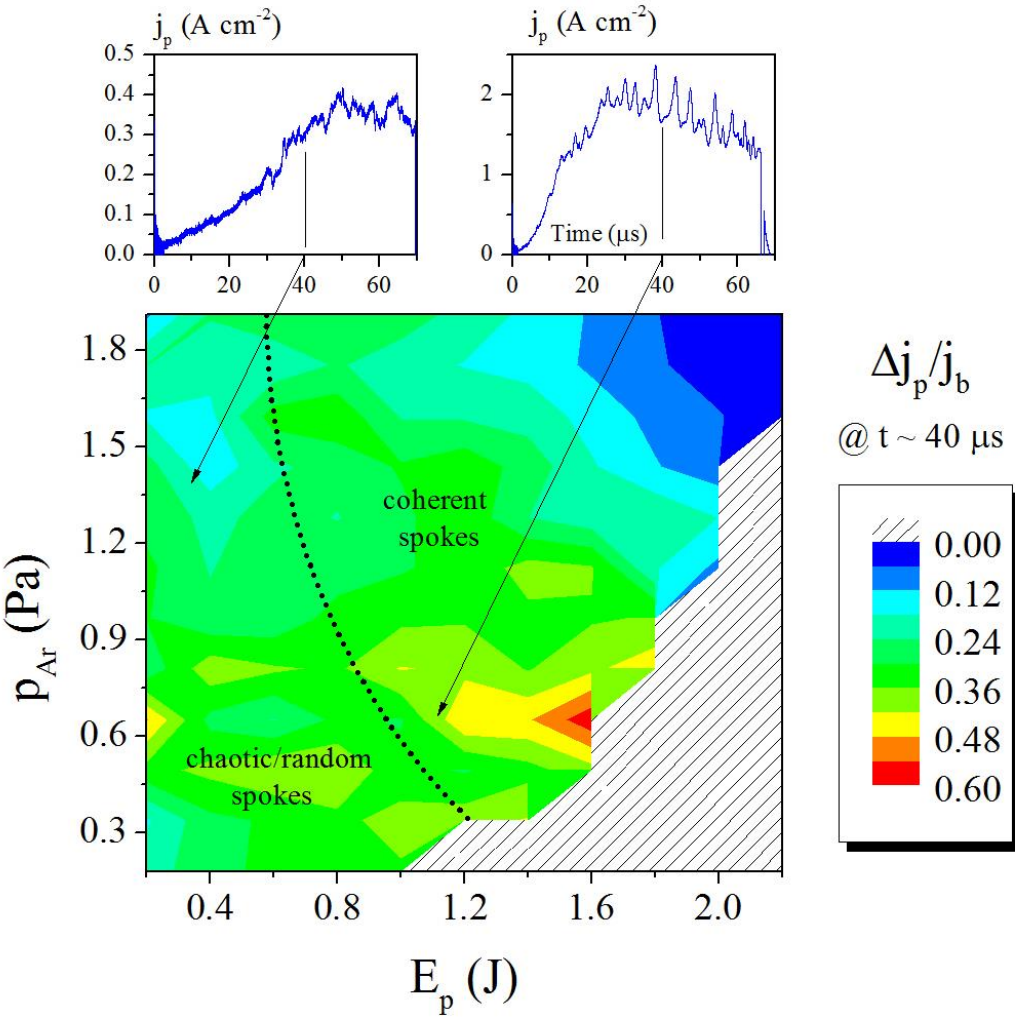

1

2

3

4 Figure 4.

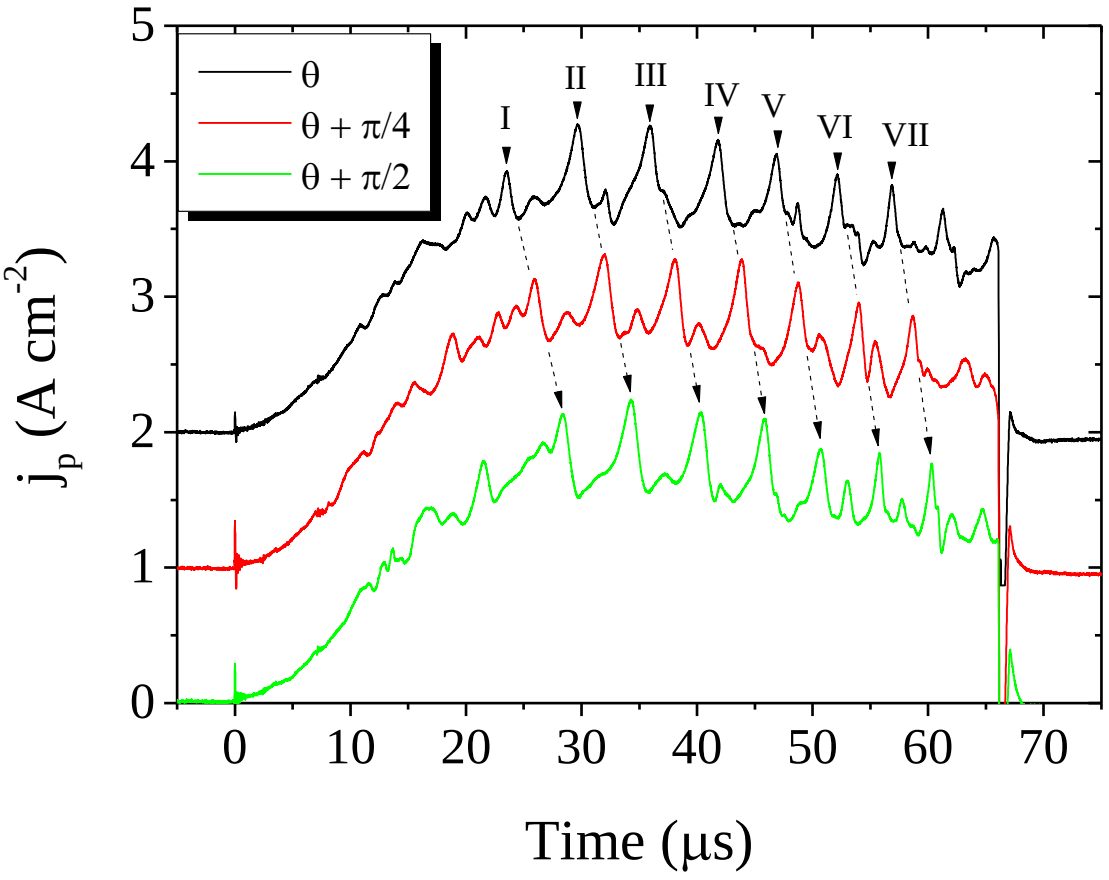
θ
θ + π/4
θ + π/2
I
II
III
IV
V
VI
VII
j_p (A cm^{-2})
Time (μs)
0
1
2
3
4
5
0
10
20
30
40
50
60
70

Figure 5.

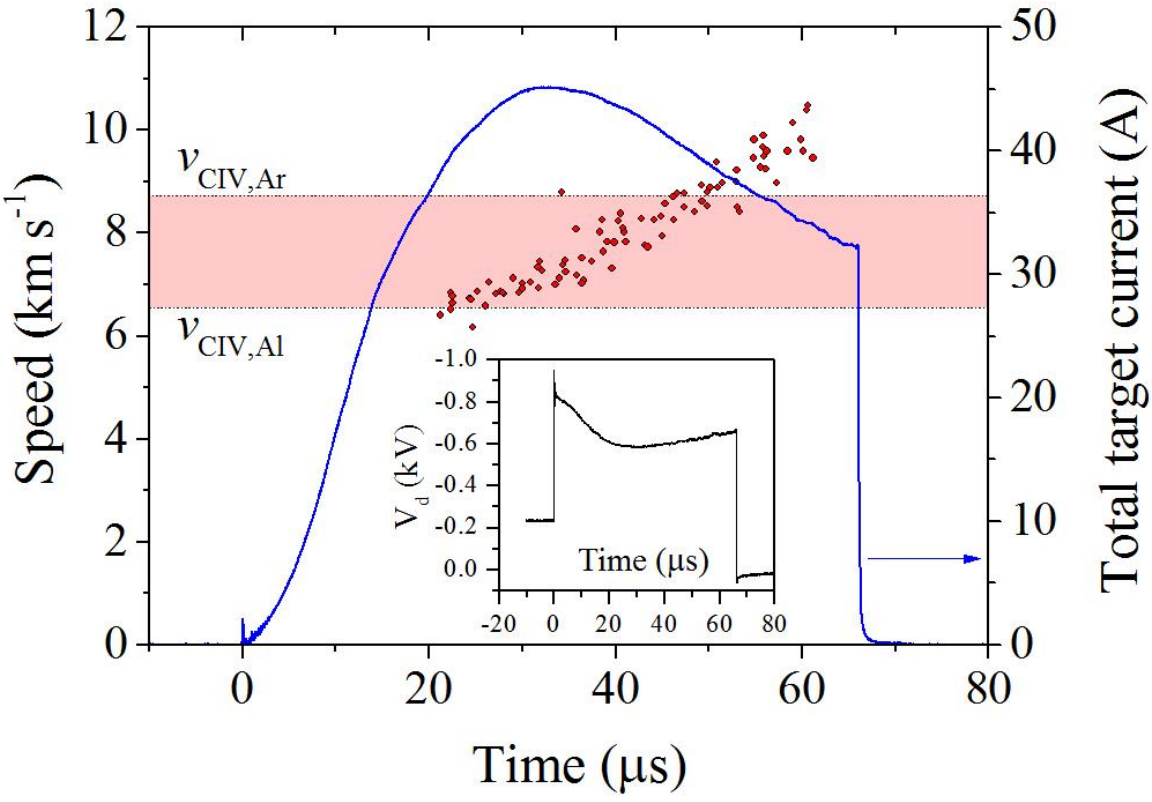
Speed (km s^{-1})
Total target current (A)
Time (μs)
$v_{CIV,Ar}$
$v_{CIV,Al}$
V_d (kV)
Time (μs)

Figure 6.

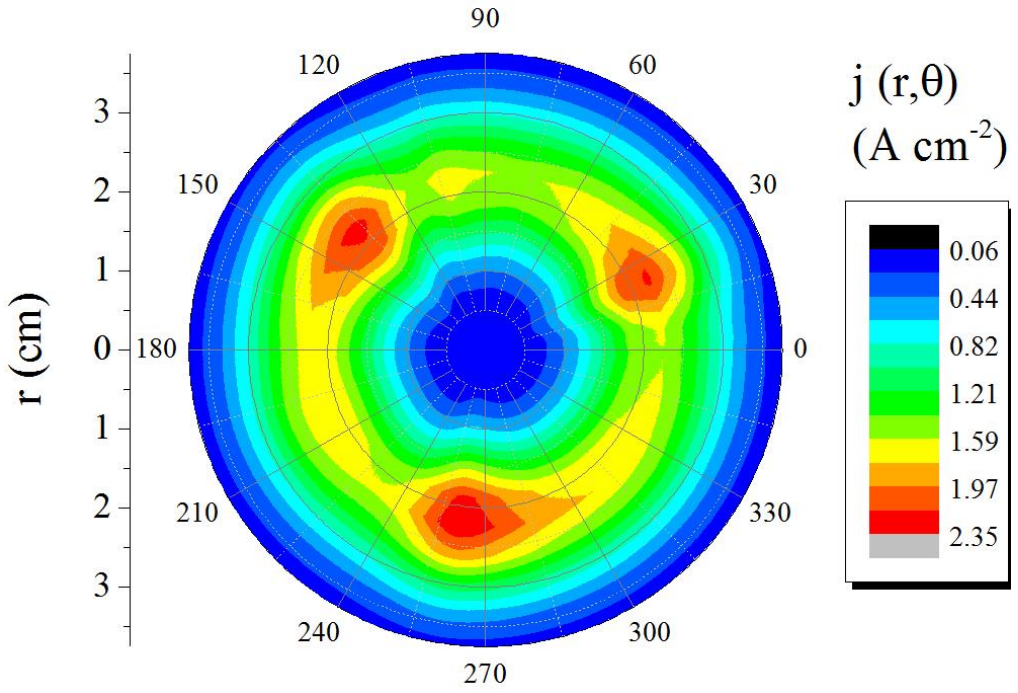
90
120
60
150
30
180
0
210
330
240
300
270
r (cm)
3
2
1
0
1
2
3
j (r,θ)
(A cm-2)
0.06
0.44
0.82
1.21
1.59
1.97
2.35

Figure 7.

Peak	τ_{AB} (μs)	τ_{BC} (μs)	τ_{avg} (μs)	ω (rad s^{-1})	v (km s^{-1})
I	2.45	2.41	2.43	3.23×10^5	6.95
II	2.29	2.36	2.33	3.37×10^5	7.26
III	2.13	2.27	2.20	3.57×10^5	7.68
IV	2.04	2.02	2.03	3.87×10^5	8.32
V	1.96	1.91	1.94	4.05×10^5	8.73
VI	1.80	1.86	1.83	4.29×10^5	9.23
VII	1.67	1.78	1.73	4.54×10^5	9.79

Table 1